NeuroImage: Clinical 25 (2020) 102112

Contents lists available at ScienceDirect

NeuroImage: Clinical

journal homepage: www.elsevier.com/locate/ynicl

Disentangling brain functional network remodeling in corticobasal syndrome – A multimodal MRI study

Tommaso Ballarini[a,*], Franziska Albrecht[a], Karsten Mueller[a], Robert Jech[c], Janine Diehl-Schmid[d], Klaus Fliessbach[e], Jan Kassubek[f], Martin Lauer[g], Klaus Fassbender[h], Anja Schneider[e], Matthis Synofzik[i,j], Jens Wiltfang[k], FTLD Consortium Germany[1], 4RTNI[2], Markus Otto[f], Matthias L Schroeter[a,b]

[a] *Max Planck Institute for Human Cognitive and Brain Sciences Leipzig, Germany*
[b] *Clinic for Cognitive Neurology, University Clinic, Leipzig, Germany*
[c] *Department of Neurology, Charles University, First Faculty of Medicine, Prague, Czech Republic*
[d] *Department of Psychiatry and Psychotherapy, Technical University of Munich, Germany*
[e] *Department of Neurodegenerative Diseases and Geriatric Psychiatry, University Bonn, Germany*
[f] *Department of Neurology, University of Ulm, Germany*
[g] *Clinic for Psychiatry, Psychosomatic medicine and Psychotherapy, University Würzburg, Germany*
[h] *Clinic for Neurology, Saarland University, Germany*
[i] *Department of Neurodegenerative Diseases, Centre for Neurology & Hertie-Institute for Clinical Brain Research, University of Tübingen, Germany*
[j] *German Center for Neurodegenerative Diseases (DZNE), Tübingen, Germany*
[k] *University Medical Center Göttingen, Germany*

ARTICLE INFO

Keywords:
Corticobasal syndrome
Imaging biomarkers
Magnetic resonance imaging
Resting-state functional connectivity
Voxel-based morphometry
Support vector machine

ABSTRACT

Objective: The clinical diagnosis of corticobasal syndrome (CBS) represents a challenge for physicians and reliable diagnostic imaging biomarkers would support the diagnostic work-up. We aimed to investigate the neural signatures of CBS using multimodal T1-weighted and resting-state functional magnetic resonance imaging (MRI).

Methods: Nineteen patients with CBS (age 67.0 ± 6.0 years; mean ± SD) and 19 matched controls (66.5 ± 6.0) were enrolled from the German Frontotemporal Lobar Degeneration Consortium. Changes in functional connectivity and structure were respectively assessed with eigenvector centrality mapping complemented by seed-based analysis and with voxel-based morphometry. In addition to mass-univariate statistics, multivariate support vector machine (*SVM*) classification tested the potential of multimodal MRI *to differentiate patients and controls*. External validity of SVM was assessed on independent CBS data from the 4RTNI database.

Results: A decrease in brain interconnectedness was observed in the right central operculum, middle temporal gyrus and posterior insula, while widespread connectivity increases were found in the anterior cingulum, medial superior-frontal gyrus and in the bilateral caudate nuclei. Severe and diffuse gray matter volume reduction, especially in the bilateral insula, putamen and thalamus, characterized CBS. SVM classification revealed that both connectivity (area under the curve 0.81) and structural abnormalities (0.80) distinguished CBS from controls, while their combination led to statistically non-significant improvement in discrimination power, questioning the additional value of functional connectivity over atrophy. SVM analyses based on structural MRI

* Corresponding author.
E-mail address: tommaso@cbs.mpg.de (T. Ballarini).

[1] Members of the German FTLD-Consortium: Sarah Anderl-Straub (Ulm), Katharina Brüggen (Rostock), Adrian Danek (LMU München), Marie Fischer (Erlangen), Hans Förstl (TU Muenchen), Anke Hammer (Erlangen), György Homola (Würzburg), Walter Just (Ulm), Marianna Kulko (Leipzig), Bernhard Landwehrmeyer (Ulm), Johannes Levin (LMU München), Albert Ludolph (Ulm), Nicolai Marroquin (Ulm), Anke Marschhauser (Leipzig), Magdalena Nagl (Ulm), Timo Oberstein (Erlangen), Maryna Polyakova (Leipzig), Hannah Pellkofer (Goettingen), Tanja Richter-Schmidinger (Erlangen), Carola Rossmeier (TU München), Katharina Schuemberg (Leipzig), Elisa Semler (Ulm), Annika Spottke (Bonn), Petra Steinacker (Ulm), Angelika Thöne-Otto (Leipzig), Ingo Uttner (Ulm), and Heike Zech (Goettingen), Holger Jahn (Hamburg), Johannes Kornhuber (Erlangen), Johannes Prudlo (Rostock).

[2] Data used in preparation of this article were obtained from the 4-Repeat Tauopathy Neuroimaging Initiative (4RTNI) database (http://4rtni-ftldni.ini.usc.edu). The investigators at 4RTNI contributed to the design and implementation of 4RTNI and/or provided data, but did not participate in analysis or writing of this report (unless otherwise listed).

https://doi.org/10.1016/j.nicl.2019.102112
Received 9 August 2019; Received in revised form 27 November 2019; Accepted 1 December 2019
Available online 02 December 2019

generalized moderately well to new data, which was decisively improved when guided by meta-analytically derived disease-specific regions-of-interest.
Conclusions: Our data-driven results show impairment of functional connectivity and brain structure in CBS and explore their potential as imaging biomarkers.

1. Introduction

Corticobasal syndrome (CBS) is an atypical parkinsonian syndrome clinically defined on the basis of motor and non-motor features (Armstrong et al., 2013; Chahine et al., 2014). Core CBS symptoms, as described in the very first cases reported (Rebeiz et al., 1968), are progressive and asymmetrical rigidity and apraxia. These are often associated with cortical manifestations – such as alien/anarchic limb and cortical sensory impairment – and with basal ganglia impairment leading to focal dystonia, tremor and bradykinesia (Armstrong et al., 2013; Boeve et al., 2003). Additionally, recent studies have moved the focus from the classical motor presentation of CBS to cognitive and behavioral symptoms (Burrell et al., 2014). In particular, impairments in multiple cognitive domains have been described, including executive functions, memory, language, visuo-spatial abilities and social cognition (Burrell et al., 2014). Of note, the previously neglected cognitive deficits can emerge with, or even precede, motor symptoms (Mathew et al., 2011; Murray et al., 2007; Parmera et al., 2016). This complex presentation makes the clinical diagnosis of CBS a challenge for physicians. Indeed, different diagnostic criteria for CBS are used across centers (Mathew et al., 2011). Post-mortem studies have shown that not only corticobasal degeneration – a tauopathy –, but also several other neuropathological substrates can cause the abovementioned CBS clinical phenotype, thus making the whole picture even more puzzling (Boeve, 2011). For example, Höglinger et al. (2017) recently reported CBS as one of the possible clinical manifestations in autopsy-confirmed progressive supranuclear palsy (Höglinger et al., 2017). Furthermore, neuropathologically confirmed corticobasal degeneration is in turn linked to different clinical presentations as reported in the diagnostic criteria (Armstrong et al., 2013).

To increase diagnostic accuracy, recent research focused on searching for novel CBS biomarkers. For example, structural T1-weighted magnetic resonance imaging (MRI) has consistently revealed gray matter decreases in patients with CBS compared to healthy controls, encompassing the basal ganglia, thalamus, insula, superior parietal cortex and frontal lobes, as summarized by Albrecht et al. (2017). In addition, *in vivo* molecular imaging studies with positron emission tomography have identified alterations in glucose metabolism in CBS (Caminiti et al., 2017; Eckert et al., 2005), as well as evidence of accumulation of β-amyloid in motor cortex, basal ganglia and corticospinal tract (Smith et al., 2017) beside expected tau protein accumulation (Kikuchi et al., 2016).

Until now, very few data have been reported on functional connectivity changes in CBS and a thorough, data-driven investigation is still missing (Bharti et al., 2017; Filippi et al., 2019; Upadhyay et al., 2017), despite it might provide valuable information (Seeley et al., 2009). Indeed, CBS, as other neurodegenerative diseases, can be conceptualized as a disconnection syndrome, where the study of functional brain connectivity represents a promising link between clinical phenotypes and underlying neuropathology (Pievani et al., 2014; Warren et al., 2013).

We believe that the identification of novel multimodal MRI-based diagnostic imaging biomarkers will lead to a better understanding and earlier and more accurate diagnosis of CBS. Therefore, we studied CBS patients and healthy controls combining resting-state functional MRI (rs-fMRI) and structural T1-weighted MRI (T1-MRI). To investigate connectivity, we applied data-driven whole-brain analysis – Eigenvector connectivity mapping (ECM) – and seed-based analysis. Additionally, we implemented an established multivariate machine learning technique, support vector machine (SVM) classification, to differentiate patients from controls based only on multimodal neuroimaging data (Ballarini et al., 2019; Bisenius et al., 2017; Dukart et al., 2011; Meyer et al., 2017; Mueller et al., 2017; Woo et al., 2017). We hypothesized that CBS, compared to controls, is characterized by widespread cortical atrophy and reductions in brain functional connectivity that can accurately distinguish CBS patients from controls at the single-subject level.

2. Materials and methods

2.1. Participants

Nineteen CBS patients (age 67.05 ± 6.03 years, mean ± SD; 12 female) and 19 healthy controls (age 66.47 ± 5.99 years; 11 female) were selected (Table 1). CBS is a rare disorder, the 19 patients were acquired over a timespan of approximately 5 years in several centers across Germany. Each patient was carefully matched with a control subject acquired on the same MRI scanner model, matching also for age and gender. All patients and seven controls were examined at different centers in the context of the German Frontotemporal Lobar Degeneration (FTLD) Consortium (http://www.ftld.de/). Six controls were recruited at the Max-Planck Institute for Human Cognitive and Brain Sciences in Leipzig, Germany, and other six at the Department of Neurology, Charles University of Prague, Czech Republic. Further details on MRI acquisition parameters are displayed in Table e-1. As expected from the sample matching procedure, no significant differences in age ($t(36) = 0.303$, $p = 0.7639$) or gender distributions ($\chi^2 = 0.11$, $p = 0.74$) were found between CBS and controls.

Cerebrospinal fluid (CSF) measures for amyloid beta 1–42, total-tau and phospho-tau were available for 14 out of 19 CBS patients. Mean and dispersion values are reported in supplementary Table e-5. Of note, only one patient showed a CSF pattern suggestive of Alzheimer's disease (McKhann et al., 2011), i.e. one marker for amyloid pathology (low amyloid-beta 1–42) and one for neuronal injury (elevated tau). Another subject presented low amyloid-beta 1–42, but normal tau levels. We decided to keep all patients in our study because (1) according to the diagnostic criteria for CBD (Armstrong et al., 2013) there is no specific pattern of these CSF markers related to the disease; (2) according to Armstrong et al. (2013), excluding amyloid positive individual might lead to miss about 13% of patients who really have the disease; (3) none of the patients clinically presented features of Alzheimer's dementia.

All CBS patients were also part of a recent study from our group based on structural MRI (Albrecht et al., 2019). The study was

Table 1
Demographic and clinical characteristics of CBS patients and controls.

	CBS	Controls
N	19	19
Age (years)	67.05 ± 6.03	66.47 ± 5.99
Gender (male/female)	7/12	8/11
Disease duration (years)	3.16 ± 2.57	–
FTLD-CDR (0–24)	6.41 ± 4.09	–
MMSE (30–0)	23.69 ± 5.00	–

Note: Mean ± SD are shown. *Best and worst possible scores for MMSE and FTLD-CDR are reported in brackets. Abbreviations: CBS corticobasal syndrome; FTLD-CDR frontotemporal lobar degeneration-clinical dementia rating scale; MMSE mini-mental state examination.*

authorized by the local ethics committees of the participating centers, in line with the Declaration of Helsinki. Participants gave written informed consent.

2.2. MRI protocols and preprocessing

Rs-fMRI (300 vol, TR = 2000 ms; TE = 30 ms) and structural T1-weighted magnetization-prepared rapid gradient-echo (MPRAGE) MRI were acquired on 3 T devices. Table e-1 reports additional information on MRI scanner types that were matched between patients and controls to reduce the variability due to the multicentric nature of the study. Note that matching for individual acquisition parameters was not always possible for all pairs of patients and controls. MRI data were processed using SPM12 (rev.12.6685), FSL (v. 5.0.9) (Jenkinson et al., 2012) and Matlab™ 9.0 (R2016 a).

Rs-fMRI images underwent SPM preprocessing with the following steps: realignment with rigid co-registration of functional volumes to the first one, slice-time correction using as reference the middle slice, and spatial normalization to the Montreal Neurological Institute (MNI) space performed via unified segmentation approach that includes bias field correction and segmentation (Ashburner and Friston, 2005). Further, images were smoothed with a Gaussian kernel (full-width-half-maximum 8 mm) to increase signal-to-noise ratio. Nuisance regression was performed including six motion parameters from the SPM realignment, as well as mean intensity signals extracted from the anatomical segmentation of white matter and cerebrospinal fluid based on each subject's T1-MRI. Finally, high-pass filtering (1/80 Hz) was applied to remove linear baseline drifts and low-frequency noise. Framewise-displacement (FD) (Power et al., 2012) was computed to assess head motion. For each participant, we computed mean FD, maximum FD and maximum FD after disregarding the largest 5% of the FD. We then compared each measure between patients and controls using two-independent sample t-tests and we did not find significant differences (Table e-2). To test the efficacy of the motion correction procedures, FD was re-computed after nuisance regression. All FD measures drastically improved in patients and controls (Figs. e-1 and e-2).

As for T1-MRI, a voxel-based morphometry (VBM) analysis (Ashburner and Friston, 2000) was performed with the Computational Anatomy Toolbox (CAT-12). Images were spatially normalized and segmented into gray matter, white matter and cerebrospinal fluid. Modulation for the amount of linear and non-linear deformation was performed, followed by smoothing with a Gaussian kernel (full-width-half-maximum 8 mm).

2.3. MRI statistical analysis

2.3.1. MRI group comparisons

ECM: ECM is a graph-theory method to investigate interconnectedness in complex networks. This concept is for example implemented by Google in the PageRank algorithm (Brin and Page, 1998) to rank websites in the search engine output. Lohmann et al. (2010) applied this approach to study brain functional interconnectedness. In brief, a brain region (node) is more important when it has many connections with other prominent nodes that are in turn linked to other heavily connected nodes. Accordingly, ECM is a good measure for the identification of brain functional hubs. We performed whole-brain voxel-wise analysis including a total of 30,110 voxels. The mask for the ECM analysis was created combining the gray matter tissue probability map from SPM (thresholded at 0.2 and smoothed with 8 mm to obtain an inclusive mask) with the functional data from patients and controls to exclude voxels containing missing values. The LIPSIA software was used for computing ECM (Lohmann et al., 2010). Blood-oxygen-level dependent (BOLD) time-courses between voxels can show both positive and, to a minor extent, negative correlations. In our study, we disregarded the negative correlations to satisfy the requirements of the Perron-Frobenius theorem, which states that a unique largest eigenvalue can be obtained only for a symmetric and positive similarity matrix (Perron, 1907). Indeed, methods to deal with negative correlations are inconsistent and their interpretation is complex (Goelman et al., 2014; Murphy et al., 2009). As a result of this analysis, a 3 D map was obtained for each subject, containing voxel-wise EC values.

CBS patients and controls were compared in a two-independent sample *t*-test in SPM. The impact of nuisance covariates on the group comparison (i.e. age, gender and scanner type) was tested via F-tests. Since no significant influence was found, we chose the simplest model excluding nuisance variables. A cluster-level correction for multiple comparisons was applied to identify significant voxels at $p < 0.05$ family-wise error (FWE) (cluster-forming threshold $p < 0.005$, $k = 50$). In order to validate the robustness of the results, the t-tests were run using a leave-one-pair out approach, i.e. running the statistical models 19 times while removing one pair of matched patient and control at a time. Finding consistent results across this procedure provides a further validation against possible confounds such as scanner/center variability and head motion. Additionally, in order to overcome the potential pitfalls of cluster-based thresholding (Eklund et al., 2016), we re-analyzed the comparison of patients and controls using the threshold free cluster enhancement (TFCE) toolbox in SPM with 5000 permutations, extent $E = 0.6$ and statistical significance threshold at $p < 0.05$ false discovery rate (FDR).

Finally, an additional ECM analysis was performed using the so-called *neg approach*, i.e. disregarding all positive correlations between BOLD time-courses and computing ECM based on the absolute values of negative correlations. Group comparisons between patients and controls were run as described above also based on these additional ECM maps.

Seed-based analysis: ECM reveals changes in general brain connectivity (e.g. hubs), but do not highlight selective connectivity changes between specific brain regions. To further explore selective connectivity changes related to the ECM comparison, we performed seed-based analysis with an in-house script running in Matlab. The seeds were placed in the peaks of the significant clusters for the group comparisons CBS > Controls and CBS < Controls based on ECM results. MNI coordinates for the nine seeds are reported in Table 2. BOLD time-courses at the selected coordinates correlated with the time-courses of all other voxels in the brain. This procedure generated, for each subject, a map with voxel-wise correlation coefficients with the seeds. We then tested between-groups differences in a two-sample *t*-test in SPM (CBS vs. Controls, $p < 0.05$ FWE at cluster level, voxel-wise cluster-forming threshold $p < 0.005$, $k = 50$). Specifically, increases in connectivity in the CBS groups were investigated from the CBS > Controls seeds and decreases of connectivity from the CBS < Controls ones. To merge together results from different seeds, the output SPM beta-images, i.e.

Table 2
Results of the eigenvector centrality group comparison.

	MNI x y z / Seeds	T	Extent	$P_{FWE\text{-}corr}$
CBS < Controls				
Cluster I	54 −19 −10	5.02	230	0.013
	54 5 −1	4.28		
	42 −13 17	4.12		
CBS > Controls				
Cluster I	6 38 41	4.44	439	0.0003
	−15 23 47	4.40		
	−18 20 14	4.15		
Cluster II	18 8 23	4.20	201	0.024
	18 53 23	4.16		
	27 23 11	4.01		

Note: Significant clusters surviving the cluster-level FWE correction for multiple comparisons in the ECM group comparison analysis are reported. The MNI coordinates were also used as seeds in the seed-based connectivity analysis. Abbreviations: CBS corticobasal syndrome; MNI Montreal Neurological Institute; FWE family-wise error.

effect size maps, were entered in a one-sample *t*-test to identify the regions where connectivity changes are consistent across the seeds. This procedure was run separately for increases and decreases in connectivity.

T1-MRI: Gray matter volume images were compared between patients and controls in a two-independent samples *t*-test, controlling for total intracranial volume, age, gender and scanner type as nuisance covariates. Results were deemed significant using a voxel-wise threshold $p < 0.005$ ($k = 50$) and cluster level correction for multiple comparisons $p < 0.05$ FWE. As for resting-state data, the comparison between CBS and controls was additionally performed using the TFCE toolbox (5000 permutations, $E = 0.6$)

2.3.2. Influence of local gray matter volume on connectivity differences

Leveraging on multimodal MRI data, we performed an additional analysis in order to disentangle the effect of atrophy on eigenvector centrality differences between patients and controls. To this aim, we used the toolbox Biological Parametric Mapping (BPM) from (Casanova et al., 2007), running in SPM8 and Matlab 7.14. Briefly, the comparison between ECM maps between patients and controls was performed entering gray matter volume images for each subject as covariate in the analysis. In order to bring images from both modalities in the same resolution, voxels in ECM maps were up-scaled to 1.5 mm^3. Results were deemed significant using a voxel-wise threshold $p < 0.005$ and cluster level correction for multiple comparisons $p < 0.05$ FWE.

2.3.3. Correlation analysis

For both ECM and VBM data, we analyzed whole-brain correlations between EC values or gray matter volume and standardized measures for disease severity, namely frontotemporal lobar degeneration-clinical dementia rating scale (FTLD-CDR) and mini-mental-state examination (MMSE). Data for MMSE and FTLD-CDR were missing, respectively, for three and two patients. In brief, ECM values and gray matter volume were separately correlated with clinical variables in the CBS group, controlling for differences in age, gender, scanner type and, only for VBM data, total intracranial volume. Significance level was set at $p < 0.05$ FWE corrected at the cluster level, with cluster forming threshold $p < 0.005$ ($k = 50$). When no significant findings were detected at the whole-brain level, correlation analyses were performed correlating the clinical variables with EC or gray matter volume values extracted from the peak MNI coordinates of the significant clusters in the group comparisons (i.e. ECM or VBM group comparisons). Correlations were assessed by two-tailed Spearman's rank correlation coefficient ($\alpha = 0.05$) using FDR correction to account for multiple comparisons.

2.3.4. MRI-based support vector machine classification

In order to ascertain the disease state from MRI data at the individual level, multimodal SVM classification was performed with PRoNTo v.2.1 (Schrouff et al., 2013). This approach is based on multivariate pattern analysis and it is inherently different from univariate statistics. We investigated the predictive value for separating patients and controls of rs-fMRI (ECM model) and T1-MRI (gray matter volume maps – VBM model) separately and combined (Combined model). To have the same number of features in structural and functional maps, as required by the PRoNTo v.2.1 software, rs-fMRI data were upscaled to a voxel resolution of 1.5 mm^3. Training was performed with a leave-one-out cross-validation. The combination of the two modalities was achieved with "simple Multiple-Kernel Learning" (sMKL) algorithm (Rakotomamonjy et al., 2008). This technique computes a single kernel for each modality and then finds their optimal combination, defining their relative importance while maximizing the margin for the classification problem. The significance of the classification accuracy was tested with a 10,000 permutation test. In order to compare if one model would outperform the others, we compared the areas under the curves (AUC) of their respective ROC curves using the non-parametric DeLong test (DeLong et al., 1988).

To further test the robustness of the classifier with changes in the cross-validation scheme, the models were re-run using 5-fold cross-validation on subject per group, instead of the leave-one-out approach. The effect of nuisance covariates was further tested. All the three models (ECM, VBM and Combined) were run controlling for either age and gender, or scanner or both, thus creating a total of 9 additional models. Both age and gender were coded using the one-hot encoding

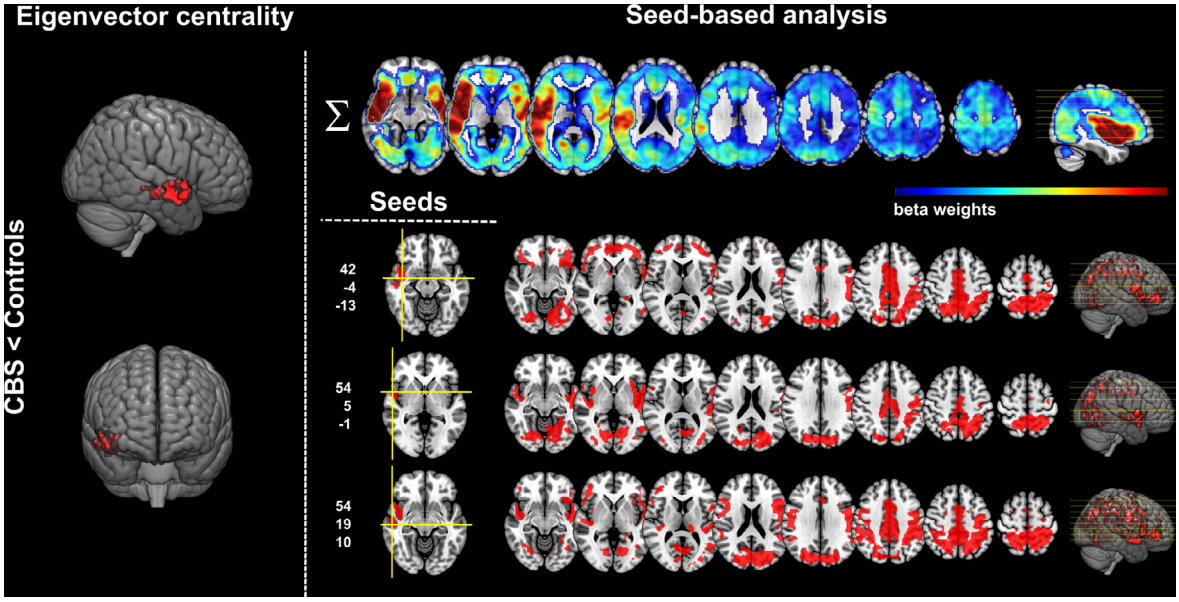

Fig. 1. Temporoparietal and insular connectivity decreases in CBS compared to controls. On the left, decreases in eigenvector centrality in patients with corticobasal syndrome compared to controls. On the right, results of the seed-based analysis showing selective connectivity decreases in patients compared to controls. MNI coordinates for all the individual seeds from the CBS < Controls group comparison are reported on the left side (x,y,z from top to bottom). The upper row shows the most consistent regions emerging from the combination of SPM beta-weights maps from different seeds. Results are shown at $p < 0.05$ FWE corrected at cluster level. Axial images are displayed in radiological convention: left brain on the right of image. Abbreviations: CBS corticobasal syndrome. (For interpretation of the references to color in this figure legend, the reader is referred to the web version of this article.)

strategy to ensure that all values in the covariates are assigned the same importance.

Finally, the external validity of the VBM model was tested on an independent dataset of CBS patients from the 4-Repeat Tauopathy Neuroimaging Initiative (4RTNI, http://4rtni-ftldni.ini.usc.edu). T1-MPRAGE MRI data acquired in different centers at 3 T devices were included for 39 patients (age: 66.2 ± 6.2, mean ± SD, 20 female) diagnosed as probable CBS-CBD subtype (Armstrong et al., 2013). Details on MRI acquisition parameters are described by Dutt et al. (2016). In brief, T1-MRI data underwent voxel-based morphometry in CAT12 as described for data from the FTLD consortium. The resulting gray matter volume images were than iteratively used as test data for the SVM based on T1-MRI only. For each new subject in the independent test set, we obtained a function value from the SVM and the corresponding class attribution (i.e. CBS patient or control). The analysis was performed either using whole-brain images or restricting feature selection based on meta-analytically derived disease-specific regions of interest (ROIs). We hypothesize that using *a priori* informed ROIs from meta-analyses might improve generalizability of the classification as already shown for several other neurodegenerative diseases (Bisenius et al., 2017; Dukart et al., 2011; Meyer et al., 2017; Mueller et al., 2017). ROIs were created based on MNI coordinates from (Albrecht et al., 2017). For each MNI coordinate, the corresponding and the contralateral regions of the AAL atlas were selected to account for potential differences in lateralization between patients. The mask is graphically sown in Fig. 6 and a list of the AAL regions is reported in supplementary Table e-6. External validation was performed only for T1-MRI data for two reasons: 1) rs-fMRI data from 4RTNI cohort present acquisition parameters very different from those applied in the study, which would lead to systematic differences in the estimated connectivity measures. 2) in our FTLD cohort, rs-fMRI did not significantly improve predictive power in the classification, as shown by statistical comparison with the DeLong test (see Results).

2.4. Data availability

Clinical and MRI data are available on reasonable request to the corresponding author. To protect anonymity, no sensitive information will be shared. MRI data will be available as preprocessed gray matter volume images or eigenvector centrality/correlation maps without personal meta-data. Data will be shared in agreement with the European General Data Protection Regulation.

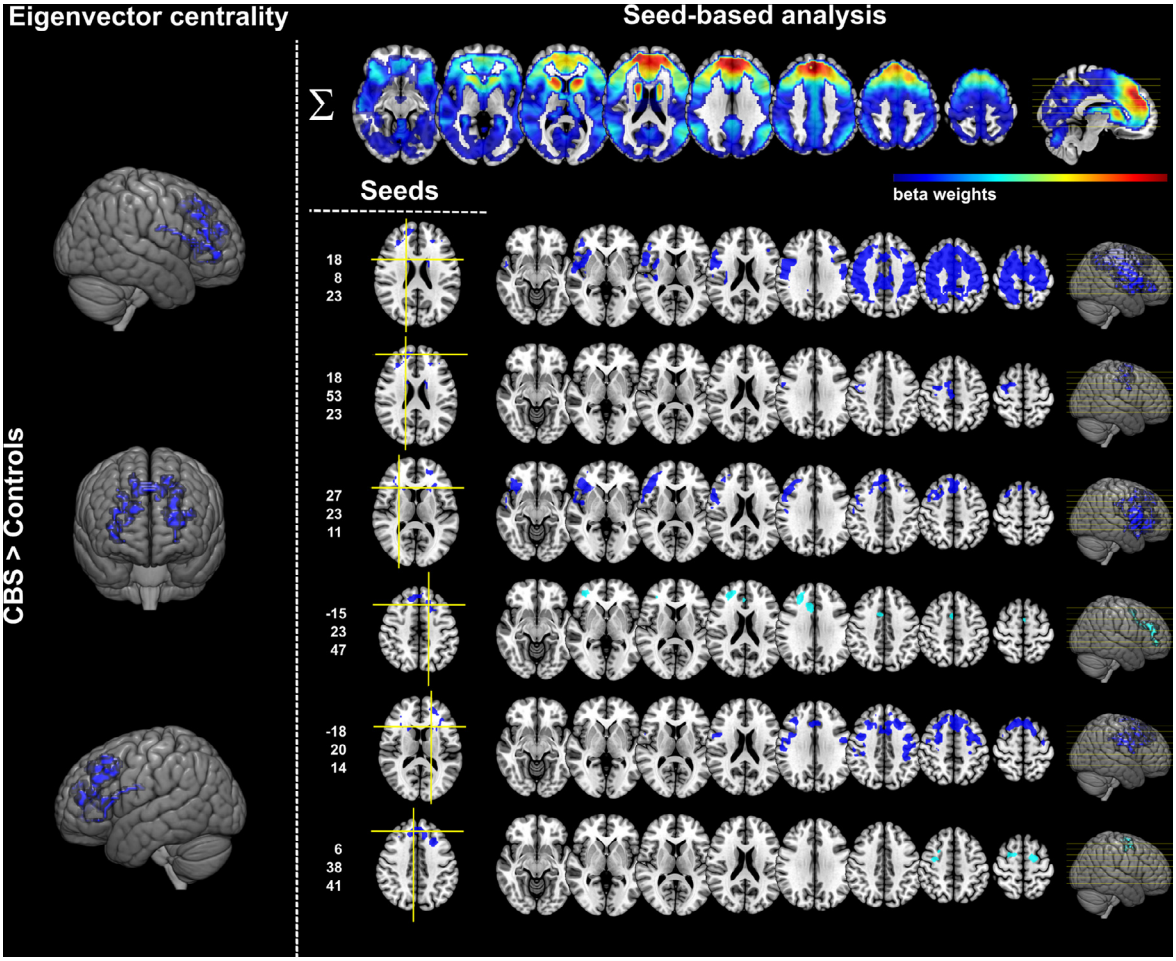

Fig. 2. Frontal and caudate connectivity increases in CBS compared to controls. On the left, frontal and caudate increases in eigenvector centrality in patients with corticobasal syndrome compared to controls. On the right, results of the seed-based analysis showing selective connectivity increases in patients compared to controls. MNI coordinates for all the individual seeds from the CBS > Controls group comparison are reported (x,y,z from top to bottom). The upper row shows the most consistent regions emerging from the combination of SPM beta-weights maps from different seeds. Results are shown at $p < 0.05$ FWE corrected at cluster level, except the light blue clusters that did not survive the correction for multiple comparisons. Axial images are displayed in radiological convention: left brain on the right of image. Abbreviations: CBS corticobasal syndrome; MNI Montreal Neurological Institute. (For interpretation of the references to color in this figure legend, the reader is referred to the web version of this article.)

3. Results

3.1. Group comparisons

ECM: As expected significant decreases in ECM were found in patients compared to controls in the right middle temporal gyrus, central operculum, planum polare and posterior insula (Fig. 1, Table 2). A similar effect was identified also in the left central operculum and transverse temporal gyrus but did not survive the correction for multiple comparisons. Remarkably, contrary to expectation, CBS patients compared to controls showed increased interconnectedness in frontal brain regions, namely in the medial superior frontal gyrus, anterior cingulate cortex, middle frontal gyri, and in the bilateral caudate nuclei (Fig. 2, Table 2). The leave-one-pair-out approach confirmed the results in all comparisons (19/19) (Fig. e-3). Additionally, re-analysis with the TFCE approach revealed ECM changes in CBS patients compared to controls very similar to those observed with cluster-based thresholding (see for details supplementary Fig. e-4).

Group comparisons of ECM maps based on negative BOLD correlations showed decreased ECM in CBS compared to controls in the bilateral sensorimotor cortex and increases in the middle cingulate gyrus (supplementary Fig. e-6).

Seed-based connectivity: For the seeds from the CBS < Controls ECM analysis, the CBS group showed markedly reduced functional connectivity from all the three seeds. In particular, the connectivity reduction involved the right insular and temporal cortex surrounding the seeds, their contralateral homologues, as well as cuneus, precuneus, middle cingulate cortex, and bilateral superior parietal cortex (Fig. 1).

Four of the six seeds from the CBS > Controls ECM comparison showed significant increases in connectivity in the seed-based analysis. The two other seeds showed similar results that did not survive the FWE correction for multiple comparisons. Altogether, CBS patients compared to controls showed increased connectivity within a fronto-caudate network involving extensively the medial frontal and anterior cingulate cortex and the bilateral caudate nuclei, as shown with one-sample *t*-test on the SPM beta-images (Fig. 2).

VBM analysis: The analysis of T1-MRI data revealed pervasive lower gray matter volume in CBS patients as compared to controls, in particular in the bilateral insulae, putamen, thalamus, in the entire cingulate cortex and widespread in cortical regions (Fig. 3). Re-analysis with the TFCE toolbox showed widespread gray matter volume loss in CBS compared to controls with a topographical distribution closely resembling the one described for the cluster-based method.

3.2. Influence of local gray matter volume on connectivity differences

The comparison of ECM maps between patients and controls, controlling for local differences in gray matter volume, revealed a pattern

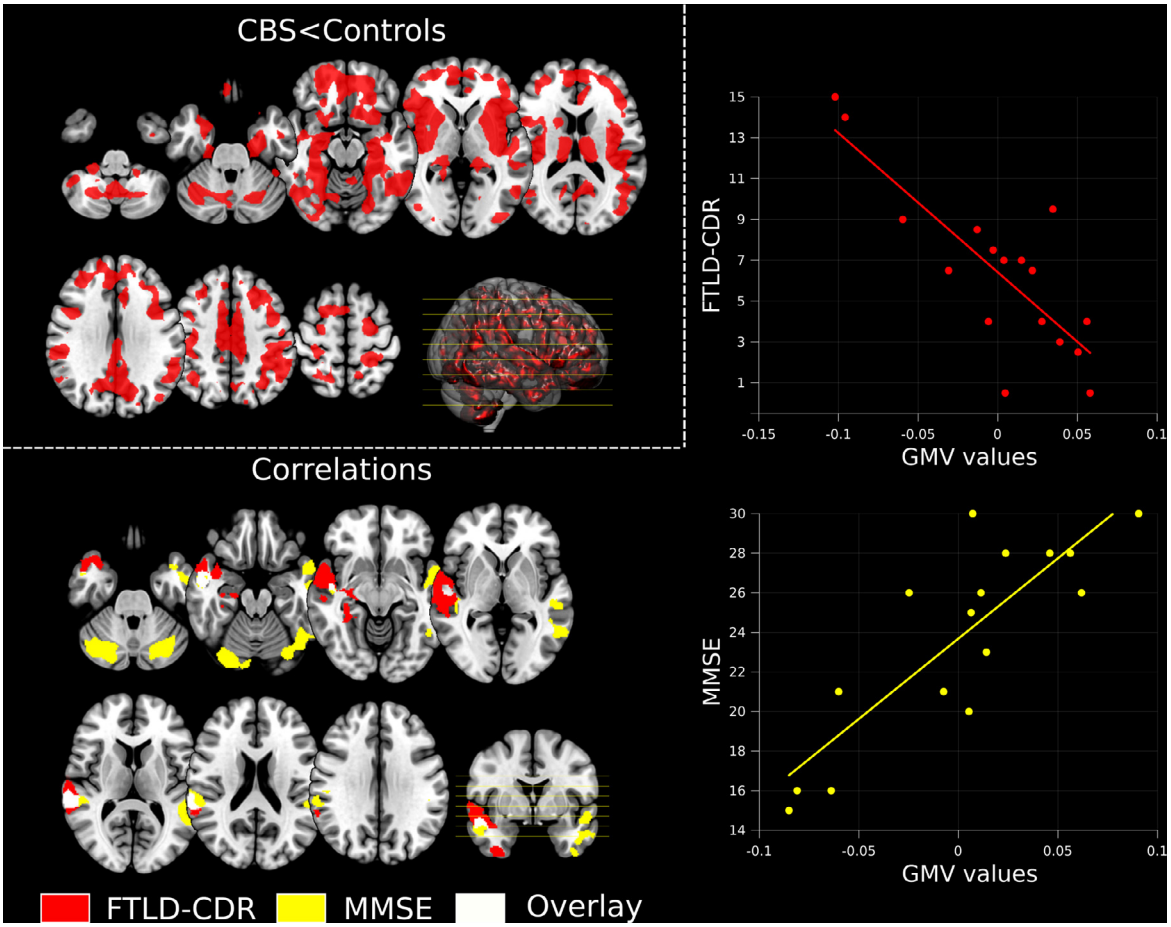

Fig. 3. Gray matter volume reductions in CBS compared to controls and correlation with disease severity. Top left quadrant: voxel-based morphometry results showing in red significant areas of structural impairment in CBS patients compared to controls. In addition, the figure displays whole-brain correlations between gray matter volume in the CBS group and standardized measures for disease severity, i.e. FTLD-CDR (red) or MMSE (yellow). The scatterplots display the correlation between test measures and gray matter volume values in the peaks of the significant clusters. The more severe the disease, the less gray matter volume is. Images are displayed in radiological convention: left brain on the right of the image. All results are shown at $p < 0.05$ FWE corrected at cluster level. Abbreviations: CBS corticobasal syndrome;FTLD-CDR frontotemporal lobar degeneration – clinical dementia rating scale; GMV gray matter volume; MMSE mini-mental state examination. (For interpretation of the references to color in this figure legend, the reader is referred to the web version of this article.)

of alterations highly comparable to the results observed in the original analysis for the CBS > Controls comparison. As for the decrease in EC in CBS < Controls, we observed a trend towards significance ($p = 0.076$) in the same cluster described in the original analysis that did not survive correction for multiple comparisons. A graphical representation is presented in supplementary Fig. e-5.

3.3. Correlation analysis

As illustrated in Fig. 3, MMSE and FTLD-CDR showed, respectively, positive and negative correlations in whole-brain VBM data, indicating lower test performance with more severe structural impairment. For MMSE, the correlation was localized in the bilateral exterior cerebellum, temporal poles, middle/superior temporal gyri, and supramarginal gyri. For FTLD-CDR the correlation analysis yielded a large cluster ranging from the right temporal pole to the middle/superior temporal and supramarginal gyri. Of note, results for MMSE and FTLD-CDR were overlapping in two clusters, located in the right temporal pole and in the superior temporal/supramarginal gyri (Fig. 3). No whole-brain correlation between clinical measures and ECM maps survived correction for multiple comparisons.

In addition, EC values in clusters from the ECM CBS > controls group comparisons positively correlated with FTLD-CDR, but not with MMSE. Note here that the FTLD-CDR is generally more sensitive for non-Alzheimer's neurodegenerative diseases, whereas the MMSE was developed for Alzheimer's dementia. Namely, a significant positive correlation was identified in the left caudate nucleus (rho = 0.641, $p = 0.027$ – FDR corrected – at MNI −18,20,14, which indicates higher caudate interconnectedness associated with a more severe clinical presentation. Moreover, FTLD-CDR scores negatively correlated with EC values in the cluster from the ECM CBS < Controls group comparison (rho = −0.634, $p = 0.027$ – FDR corrected – at MNI 54,5,−1), suggesting a more severe clinical presentation with lower right temporal/insular interconnectedness (Fig. 4).

3.4. Support vector machine classification

SVM analysis achieved good classification for both VBM and ECM models (Fig. 5). Fifteen CBS patients ($p = 0.006$) and 15 controls ($p = 0.007$) were correctly classified based only on structural data, thus with an overall balanced accuracy (BA) of 78.95% ($p = 0.002$, area under the curve, AUC = 0.80). ECM maps distinguished 14 CBS patients ($p = 0.026$) and 15 controls ($p = 0.011$), reaching an overall BA of 76.32% ($p = 0.004$, AUC = 0.81). Combining both modalities via MKL, the overall performance of the classifier increased to 84.21% ($p = 0.0001$, AUC = 0.87), correctly recognizing 16 patients ($p = 0.002$) and 16 controls ($p = 0.001$). However, the nonparametric comparison of AUCs using the DeLong test did not reveal statistically significant differences between the three models. In particular, the combined model did not outperform neither VBM alone ($p = 0.24$), nor the ECM model ($p = 0.34$). Complete output of the DeLong test is shown in supplementary Table e-5. Changes in the cross-validation had the following effects on model performance: Moderate decreased performance for the ECM model (AUC = 0.79, BA = 71.05%), increased performance for the VBM model (AUC = 0.84, BA = 84.21%) and no effect on the combined model (AUC = 0.88, BA = 84.21%). Hence, the same pattern was detected: Lowest accuracy in ECM maps, better in VBM maps, best accuracy in combined approach. The effects of covariates are descried in details in the supplementary Table e-3.

Finally, the presented VBM model showed moderate generalizability to independent data, correctly classifying 67% of new CBS whole-brain images. Notably, when using meta-analytically derived disease-specific ROIs, generalizability was higher, with 79% of new CBS patients correctly identified. Results of the external validation are shown in Fig. 6.

4. Discussion

In the present study, we provide new insights into brain functional and structural changes that characterize CBS. In sum, we show that CBS is associated with functional connectivity alterations, including both decreases in right temporo-parietal and insular regions and, remarkably, increases in a frontal network encompassing medial frontal and anterior cingulate cortex, and the bilateral caudate nuclei. Moreover, we identified brain structural abnormalities in the insula, putamen, thalamus and widespread cortical regions. Both T1-MRI and rs-fMRI independently yielded a good discrimination power to distinguish CBS patients from controls, and slightly more when combined in a single model (over 80% balanced accuracy). However, differences between the three models were not statistically significant, hence undermining the additional benefit of including rs-fMRI data for diagnostic purposes. T1-MRI data alone generalized moderately well to independent data from an external cohort. Of note, guiding feature selection with meta-analytically defined disease-specific ROIs improved generalizability. This finding is in agreement with other studies investigating several other neurodegenerative diseases and showing that

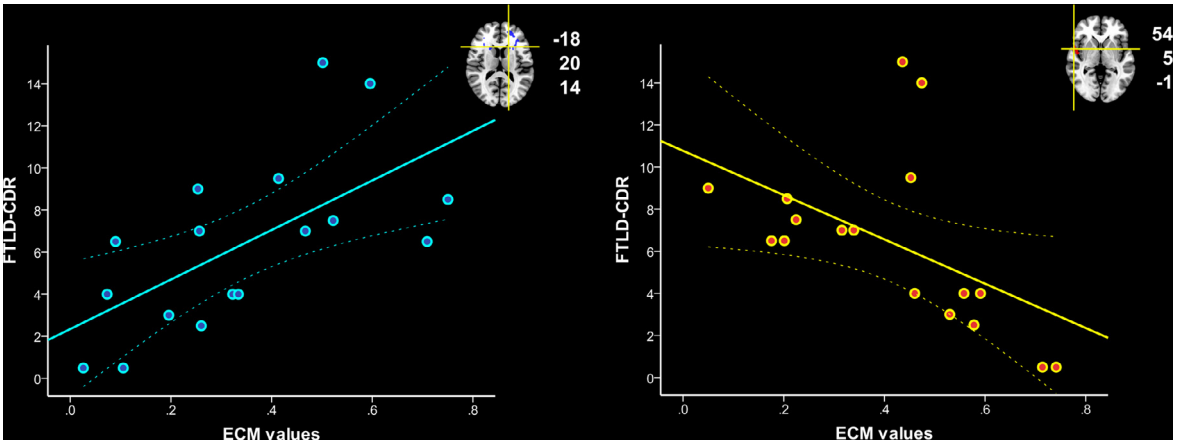

Fig. 4. Correlations between eigenvector centrality changes in CBS and disease severity. Positive and negative Spearman's correlations between FTLD-CDR, as proxy for disease severity, and eigenvector centrality in the significant clusters from the ECM CBS > controls comparison. The more severe the disease, the lower the interconnectedness in the right temporal/insular cortex, and the higher the interconnectedness in left caudate nucleus, suggesting proportional connectivity changes with disease severity and, potentially, brain compensation. MNI coordinates for the clusters are reported on the side of each scatterplot. Dotted lines represent 95% confidence intervals. Abbreviations: CBS corticobasal syndrome; ECM eigenvector centrality mapping; FTLD-CDR frontotemporal lobar degeneration – clinical dementia rating scale.

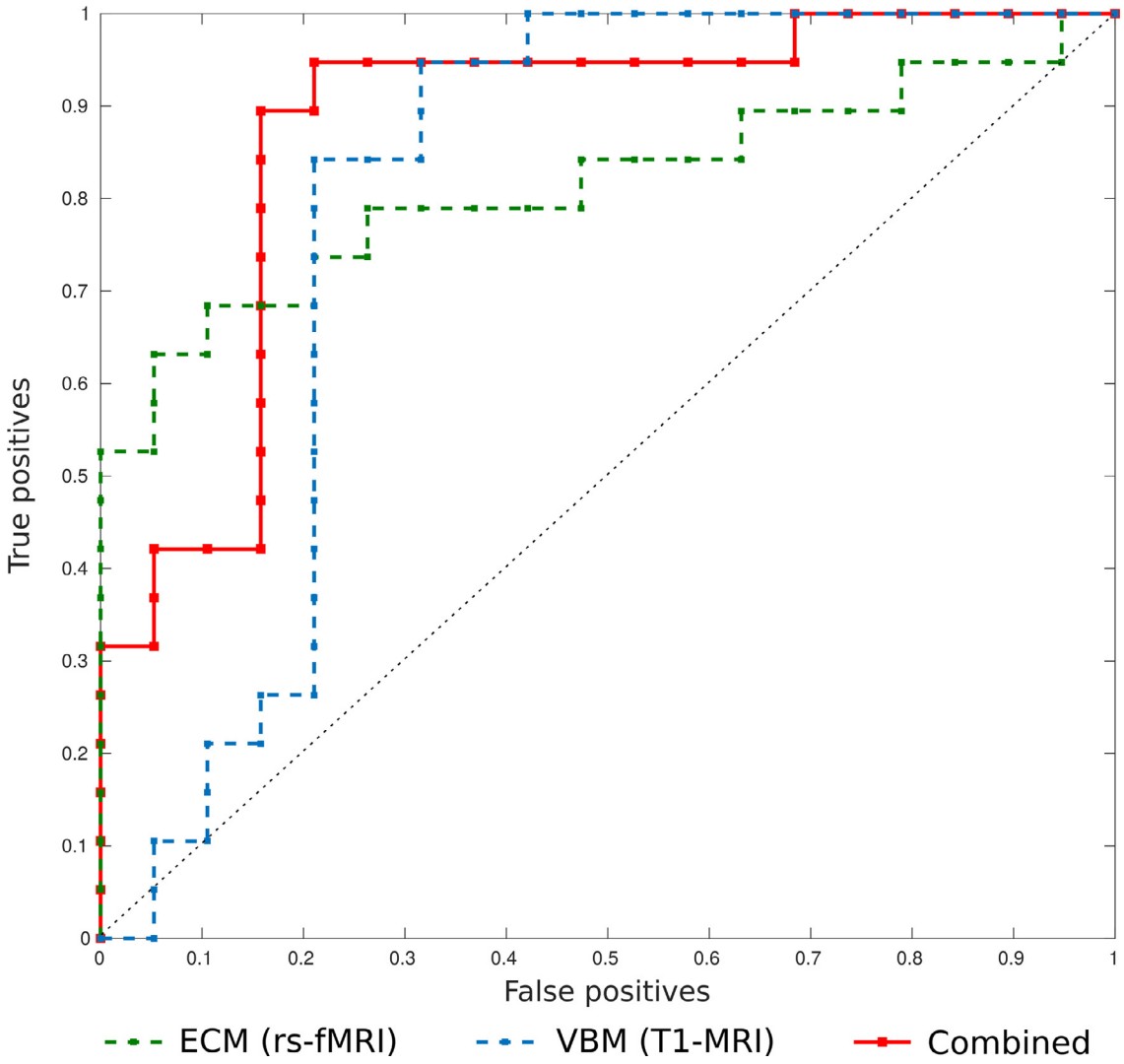

Fig. 5. Results of support vector machine classification based on MRI imaging markers. Receiver operating characteristic (ROC) curves for differentiating patients with corticobasal syndrome and healthy controls based on MRI data. The areas under the curve (AUC) for voxel-based morphometry, eigenvector centrality mapping and their combination are, respectively, 0.80, 0.81 and 0.87. Abbreviations: ECM eigenvector centrality mapping; rs-fMRI resting state-functional magnetic resonance imaging; SVM support vector machine; VBM voxel-based morphometry. (For interpretation of the references to color in this figure legend, the reader is referred to the web version of this article.)

ROIs defined in independent cohorts by systematic and quantitative meta-analyses can improve classification accuracy for diagnosis and differential diagnosis in imaging data (Bisenius et al., 2017; Dukart et al., 2011; Meyer et al., 2017; Mueller et al., 2017). Concerning rs-fMRI, our multicentric study included, to our knowledge, the largest patient cohort so far. Moreover, the application of data-driven ECM analysis gives an unbiased perspective on brain functional interconnectedness.

We analyzed whole-brain ECM changes in CBS to avoid any *a priori* assumptions. ECM analysis revealed decreased interconnectedness in right temporo-parietal and posterior insular cortex, as well as increases in frontal cortex and caudate nuclei in CBS. Seed-based analysis showed that decreases in ECM in CBS compared to controls were related to diffuse functional connectivity decline with temporo-parietal associative cortices, middle cingulate cortex and precuneus. In addition, ECM increases were associated with functional connectivity increases in a fronto-caudate network. Consistent with our results, Bharti et al. (2017) found both decreases and increases in resting-state functional connectivity in CBS compared to controls, using independent component analysis. Specifically, the CBS group showed increased within-network connectivity in regions of the default mode network, in the cerebellum, in the sensorimotor, executive control and insula networks. Between-network connectivity was lower in CBS compared to controls between the lateral visual and auditory networks and higher between salience and executive control networks. A similar investigation from the same research group (Upadhyay et al., 2017) applied seed-based analysis to rs-fMRI data from CBS and found, in comparison to controls, decreases and increases in functional connectivity, respectively when placing the seeds in the thalamus or in the dentate nucleus.

Increases in functional connectivity are a common finding not only in CBS, but also in other neurodegenerative and neuropsychiatric disorders (Greicius, 2008). The correlation analysis revealed an association between more severe disease presentation (i.e. higher FTLD-CDR scores) and lower eigenvector centrality in the right temporal cortex, as well as increased interconnectedness in left caudate nucleus. This finding suggests a progressive connectivity alteration in CBS and, potentially, a compensatory meaning of the connectivity increases. This assumption might be further supported by the fact that increased connectivity in CBS correlated with FTLD-CDR scores in contrast to atrophy. Decreases in CBS' brain connectivity instead coincided regionally with atrophy regarding correlation with the FTLD-CDR as measure of disease severity. However, additional explanations are that

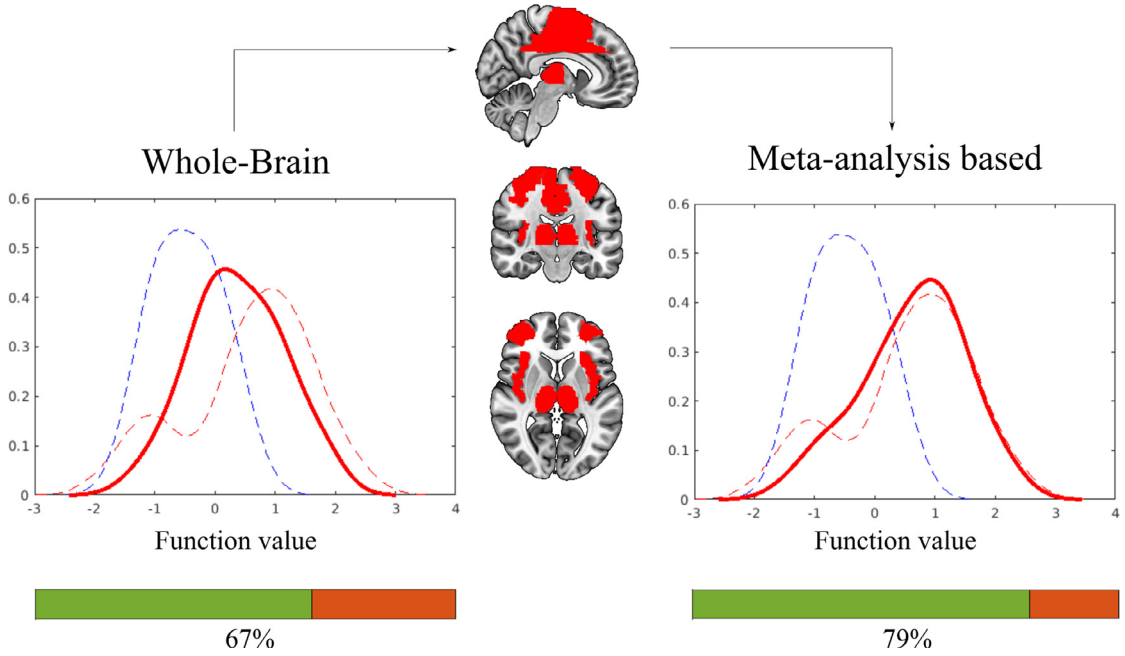

Fig. 6. External validation of SVM model based on T1-MRI. Histogram plots display the function value distributions derived from the SVM based on T1-MRI data. Dashed lines represent function values for controls (blue) and patients (red) based on whole-brain SVM analysis. The continuous red line represents the distribution of function values for the new independent cohort of 39 CBS patients. The use of meta-analytically derived regions of interests leads to improved generalization of the SVM classifier to new data. Color bars show the proportion of correctly classified CBS patients from the new cohort for both whole brain and meta-analysis guided models. (For interpretation of the references to color in this figure legend, the reader is referred to the web version of this article.)

increases in connectivity might be a sign of pathological changes within these networks or the consequence of distant pathological alterations (so called diaschisis effect). Our findings are in agreement with other studies in Alzheimer's disease and behavioral variant frontotemporal dementia, where pathological alterations in one network (e.g. the default mode) might lead to aberrant reorganization of anti-correlated networks (e.g. the anterior salience network) (Zhou et al., 2010). Hillary et al. (2015), based on the revision of 126 functional connectivity studies, proposed that hyperconnectivity is an essential and frequent response to neurological diseases. Specifically, they propose that increased connectivity has most likely a multifactorial origin, including the role of the impaired brain regions in large-scale networks and the accessibility of local and global connections (Hillary et al., 2015).

As for T1-MRI data, our results are consistent with previous studies showing severe and widespread cortical atrophy in CBS (Albrecht et al., 2019), as recently quantitatively summarized in a meta-analysis (Albrecht et al., 2017). Importantly, structural brain changes significantly correlated with both MMSE and FTLD-CDR measures. As expected, more severe gray matter volume reduction, i.e. atrophy, was associated with worse disease severity. Results for the two measures overlapped in two clusters located in the right temporal gyrus and in the superior temporal/supramarginal gyri, indicating these brain regions as hotspots of the disease, although one has to take into account the heterogeneity of both MMSE and FTLD-CDR measures (assessing cognitive, behavioral and functional symptoms).

The interrelationship between structural and functional brain changes is a general question, when exploring functional networks in neurodegeneration and here we addressed it using Biological Parametric Mapping (Casanova et al., 2007). Of note, our results show that local atrophy, although severe and widespread, does not have a significant impact on the described eigenvector centrality alterations in CBS.

By implementing a SVM approach to our data, we were able to show the potential of brain structural and functional alterations in distinguishing CBS patients from controls at the single-subject level. Both models alone performed moderately well, while their combination led to a slight but statistically non-significant improvement in discrimination power. Moreover, despite resting-state networks are consistent across subjects (Damoiseaux et al., 2006) and are known to be altered in several diseases (Greicius, 2008), a recent meta-analysis showed a modest test-retest reliability of functional connectivity measures (Noble et al., 2019). Therefore, also considering the technical limitations in smaller clinical settings, we suggest that T1-MRI might be a better candidate for future clinical applications. Along this line, previous studies applied SVM for the automatic classification of neurodegenerative diseases using MRI structural data from different centers and MRI devices showing reasonably robust performances (Klöppel et al., 2008; Koikkalainen et al., 2016). Further supporting this view, we report a fair generalizability of SVM results on a completely independent dataset of CBS patients, especially when feature selection was *a priori* informed by ROIs defined from meta-analyses of previous VBM studies in CBS (Albrecht et al., 2017). However, the usefulness of structural changes alone as specific CBS imaging markers might be hampered by the fact that partially similar structural alterations have been found in other neurodegenerative diseases, such as behavioral variant frontotemporal dementia and Alzheimer's disease (Albrecht et al., 2017).

Combining T1-MRI data with meta-analytically derived disease-specific neural networks might generally improve diagnosis and differential diagnosis as previously shown also for other several neurodegenerative diseases beside CBS (Bisenius et al., 2017; Dukart et al., 2011; Meyer et al., 2017; Mueller et al., 2017). We believe that combining T1-MRI data with additional biomarkers (e.g. from cerebrospinal fluid) and clinical information would improve the differential diagnosis. Moreover, we propose that the training of similar machine learning models in larger CBS patient cohorts would lead to better classification accuracy and might eventually lead to the inclusion of new supportive imaging markers in the CBS diagnostic criteria, as it has already happened for other neurodegenerative diseases (Dubois et al., 2010; Gorno-Tempini et al., 2011).

4.1. Limitations

With this study we aimed at identifying diagnostic imaging biomarkers for clinically defined CBS. Consequently, we did not distinguish between different underlying neuropathological profiles of CBS, although known to potentially influence atrophy patterns (Whitwell et al., 2010) and clinical presentation (Lee et al., 2011). Here we reported CSF data for 14 out of 19 CBS patients, showing that only in one case values compatible with Alzheimer' disease were found. However, at the moment being, no specific CSF biomarkers have been included in the diagnostic criteria for CBS (Armstrong et al., 2013), thus limiting the usefulness of this information. Additional studies with larger patient cohorts and autopsy-proven cases will be crucial to further disentangle this aspect. As abovementioned, differential diagnosis based on MRI biomarkers is another topic in need for further investigation. This still represents a tough challenge in the clinical workup, for example when differentiating CBS from other parkinsonian or FTLD syndromes, especially in early disease stages. The addition of disease control groups will be needed to test specificity of our finding for CBS. Finally, in this study we implemented ECM as measure of brain functional network organization at rest. However, different methodological approaches might provide further insight into functional network changes in CBS and potentially lead to a different performance as diagnostic marker.

4.2. Conclusion

In conclusion, we described brain structural and novel data-driven functional connectivity abnormalities associated with CBS. In addition to the previously described structural brain changes, we contribute evidence for intriguing characteristic functional connectivity alterations in CBS. We further compared measures of connectivity and atrophy as potential supportive MRI-based imaging markers for *differentiating CBS patients and controls*. Overall, our results suggest that structural MRI is a promising candidate imaging marker for CBS and does not benefit from inclusion of additional rs-fMRI information.

Funding

This work was supported by the German Federal Ministry of Education and Research (BMBF) by a grant given to the German FTLD Consortium (grant number FKZ O1GI1007 A), by the Parkinson's Disease Foundation (grant number PDF-IRG-1307), by the Michael Fox Foundation (grant number 11362), by the German Research Foundation (DFG, SCHR 774/5-1), by the Czech Science Foundation (GACR 16-13323 S), and by the Charles University, Czech Republic (project: Progres Q27/LF1). Additionally, data collection and sharing for 4RTNI data was funded by the 4-Repeat Tauopathy Neuroimaging Initiative (4RTNI) (National Institutes of Health Grant R01 AG038791) and through generous contributions from the Tau Research Consortium. The study is coordinated through the University of California, San Francisco, Memory and Aging Center. 4RTNI data are disseminated by the Laboratory for Neuro Imaging at the University of Southern California.

CRediT authorship contribution statement

Tommaso Ballarini: Conceptualization, Methodology, Formal analysis, Writing - original draft, Visualization. **Franziska Albrecht:** Writing - review & editing. **Karsten Mueller:** Conceptualization, Methodology, Writing - review & editing. **Robert Jech:** Investigation, Writing - review & editing. **Janine Diehl-Schmid:** Investigation, Writing - review & editing. **Klaus Fliessbach:** Writing - review & editing. **Jan Kassubek:** Writing - review & editing. **Martin Lauer:** Writing - review & editing. **Klaus Fassbender:** Writing - review & editing. **Anja Schneider:** Writing - review & editing. **Matthis Synofzik:** Writing - review & editing. **Jens Wiltfang:** Writing - review & editing. **Markus Otto:** Writing - review & editing, Supervision, Funding acquisition. **Matthias L Schroeter:** Conceptualization, Investigation, Methodology, Writing - review & editing, Supervision, Funding acquisition.

Declaration of Competing Interest

The authors report no competing interests.

Supplementary materials

Supplementary material associated with this article can be found, in the online version, at doi:10.1016/j.nicl.2019.102112.

References

Albrecht, F., Bisenius, S., Schaack, R.M., Neumann, J., Schroeter, M.L., 2017. Disentangling the neural correlates of corticobasal syndrome and corticobasal degeneration with systematic and quantitative ALE meta-analyses. NPJ Parkinson's Dis. 3, 12.

Albrecht, F., Mueller, K., Ballarini, T., Lampe, L., Diehl-Schmid, J., Fassbender, K., Fliessbach, K., Jahn, H., Jech, R., Kassubek, J., 2019. Unraveling corticobasal syndrome and alien limb syndrome with structural brain imaging. Cortex 117, 33–40.

Armstrong, M.J., Litvan, I., Lang, A.E., Bak, T.H., Bhatia, K.P., Borroni, B., Boxer, A.L., Dickson, D.W., Grossman, M., Hallett, M., 2013. Criteria for the diagnosis of corticobasal degeneration. Neurology 80, 496–503.

Ashburner, J., Friston, K.J., 2000. Voxel-based morphometry–the methods. Neuroimage 11, 805–821.

Ashburner, J., Friston, K.J., 2005. Unified segmentation. Neuroimage 26, 839–851.

Ballarini, T., Mueller, K., Albrecht, F., Růžička, F., Bezdicek, O., Růžička, E., Roth, J., Vymazal, J., Jech, R., Schroeter, M.L., 2019. Regional gray matter changes and age predict individual treatment response in Parkinson's disease. NeuroImage Clin. 21, 101636.

Bharti, K., Bologna, M., Upadhyay, N., Piattella, M.C., Suppa, A., Petsas, N., Giannì, C., Tona, F., Berardelli, A., Pantano, P., 2017. abnormal resting-state functional connectivity in progressive supranuclear palsy and corticobasal syndrome. Front. Neurol. 8, 248.

Bisenius, S., Mueller, K., Diehl-Schmid, J., Fassbender, K., Grimmer, T., Jessen, F., Kassubek, J., Kornhuber, J., Landwehrmeyer, B., Ludolph, A., 2017. Predicting primary progressive aphasias with support vector machine approaches in structural MRI data. NeuroImage Clin. 14, 334–343.

Boeve, B.F., 2011. The multiple phenotypes of corticobasal syndrome and corticobasal degeneration: implications for further study. J. Mol. Neurosci. 45, 350.

Boeve, B.F., Lang, A.E., Litvan, I., 2003. Corticobasal degeneration and its relationship to progressive supranuclear palsy and frontotemporal dementia. Ann. Neurol. 54.

Brin, S., Page, L., 1998. The anatomy of a large-scale hypertextual WEB search engine. Comput. Netw. Isdn Syst. 30, 107–117.

Burrell, J.R., Hodges, J.R., Rowe, J.B., 2014. Cognition in corticobasal syndrome and progressive Supranuclear palsy: a review. Mov. Disord. 29, 684–693.

Caminiti, S., Alongi, P., Majno, L., Volonte, M., Cerami, C., Gianolli, L., Comi, G., Perani, D., 2017. Evaluation of an optimized [18 F] fluoro-deoxy-glucose positron emission tomography voxel-wise method to early support differential diagnosis in atypical Parkinsonian disorders. Eur. J. Neurol. 24, 687.

Casanova, R., Srikanth, R., Baer, A., Laurienti, P.J., Burdette, J.H., Hayasaka, S., Flowers, L., Wood, F., Maldjian, J.A., 2007. Biological parametric mapping: a statistical toolbox for multimodality brain image analysis. Neuroimage 34, 137–143.

Chahine, L.M., Rebeiz, T., Rebeiz, J.J., Grossman, M., Gross, R.G., 2014. Corticobasal syndrome: five new things. Neurol. Clin. Pract. 4, 304–312.

Damoiseaux, J.S., Rombouts, S., Barkhof, F., Scheltens, P., Stam, C.J., Smith, S.M., Beckmann, C.F., 2006. Consistent resting-state networks across healthy subjects. Proc. Natl. Acad. Sci. 103, 13848–13853.

DeLong, E., DeLong, D., Clarke-Pearson, D., 1988. Comparing the areas under two or more correlated receiver operating characteristic curves. A nonparametric approach. Biometrics 44, 837–845.

Dubois, B., Feldman, H.H., Jacova, C., Cummings, J.L., DeKosky, S.T., Barberger-Gateau, P., Delacourte, A., Frisoni, G., Fox, N.C., Galasko, D., 2010. Revising the definition of Alzheimer's disease: a new lexicon. Lancet Neurol. 9, 1118–1127.

Dukart, J., Mueller, K., Horstmann, A., Barthel, H., Möller, H.E., Villringer, A., Sabri, O., Schroeter, M.L., 2011. Combined evaluation of FDG-PET and MRI improves detection and differentiation of dementia. PLoS ONE 6, e18111.

Dutt, S., Binney, R.J., Heuer, H.W., Luong, P., Attygalle, S., Bhatt, P., Marx, G.A., Elofson, J., Tartaglia, M.C., Litvan, I., 2016. Progression of brain atrophy in PSP and CBS over 6 months and 1 year. Neurology 87 (19).

Eckert, T., Barnes, A., Dhawan, V., Frucht, S., Gordon, M.F., Feigin, A.S., Eidelberg, D., 2005. FDG PET in the differential diagnosis of Parkinsonian disorders. Neuroimage 26, 912–921.

Eklund, A., Nichols, T.E., Knutsson, H., 2016. Cluster failure: why fMRI inferences for spatial extent have inflated false-positive rates. Proc. Natl. Acad. Sci. 113, 7900–7905.

Filippi, M., Sarasso, E., Agosta, F., 2019. Resting-state functional mri in parkinsonian syndromes. 6, 104–117.
Goelman, G., Gordon, N., Bonne, O., 2014. Maximizing negative correlations in resting-state functional connectivity MRI by time-lag. PLoS One 9, e111554.
emsp14, alGorno-Tempini, M.L., Hillis, A.E., Weintraub, S., Kertesz, A., Mendez, M., Cappa, S.e., Ogar, J., Rohrer, J., Black, S., Boeve, B.F., 2011. Classification of primary progressive aphasia and its variants. Neurology 76, 1006–1014.
Greicius, M., 2008. Resting-state functional connectivity in neuropsychiatric disorders. Curr. Opin. Neurol. 21, 424–430.
Hillary, F.G., Roman, C.A., Venkatesan, U., Rajtmajer, S.M., Bajo, R., Castellanos, N.D.J. N., 2015. Hyperconnectivity is a fundamental response to neurological disruption. 29, 59.
Höglinger, G.U., Respondek, G., Stamelou, M., Kurz, C., Josephs, K.A., Lang, A.E., Mollenhauer, B., Müller, U., Nilsson, C., Whitwell, J.L., Arzberger, T., Englund, E., Gelpi, E., Giese, A., Irwin, D.J., Meissner, W.G., Pantelyat, A., Rajput, A., van Swieten, J.C., Troakes, C., Antonini, A., Bhatia, K.P., Bordelon, Y., Compta, Y., Corvol, J.-C., Colosimo, C., Dickson, D.W., Dodel, R., Ferguson, L., Grossman, M., Kassubek, J., Krismer, F., Levin, J., Lorenzl, S., Morris, H.R., Nestor, P., Oertel, W.H., Poewe, W., Rabinovici, G., Rowe, J.B., Schellenberg, G.D., Seppi, K., van Eimeren, T., Wenning, G.K., Boxer, A.L., Golbe, L.I., Litvan, I., Movement Disorder Society-endorsed, P.S.P.S.G., 2017. Clinical diagnosis of progressive supranuclear palsy: the movement disorder society criteria. Mov. Disord. 32, 853–864 Official journal of the Movement Disorder Society.
Jenkinson, M., Beckmann, C.F., Behrens, T.E., Woolrich, M.W., Smith, S.M., 2012. Fsl. Neuroimage 62, 782–790.
Kikuchi, A., Okamura, N., Hasegawa, T., Harada, R., Watanuki, S., Funaki, Y., Hiraoka, K., Baba, T., Sugeno, N., Oshima, R., 2016. In vivo visualization of tau deposits in corticobasal syndrome by 18 F-THK5351 PET. Neurology 87, 2309–2316.
Klöppel, S., Stonnington, C.M., Chu, C., Draganski, B., Scahill, R.I., Rohrer, J.D., Fox, N.C., Jack Jr, C.R., Ashburner, J., Frackowiak, R.S., 2008. Automatic classification of MR scans in Alzheimer's disease. Brain 131, 681–689.
Koikkalainen, J., Rhodius-Meester, H., Tolonen, A., Barkhof, F., Tijms, B., Lemstra, A.W., Tong, T., Guerrero, R., Schuh, A., Ledig, C., 2016. Differential diagnosis of neurodegenerative diseases using structural MRI data. NeuroImage Clin. 11, 435–449.
Lee, S.E., Rabinovici, G.D., Mayo, M.C., Wilson, S.M., Seeley, W.W., DeArmond, S.J., Huang, E.J., Trojanowski, J.Q., Growdon, M.E., Jang, J.Y., 2011. Clinicopathological correlations in corticobasal degeneration. Ann. Neurol. 70, 327–340.
Lohmann, G., Margulies, D.S., Horstmann, A., Pleger, B., Lepsien, J., Goldhahn, D., Schloegl, H., Stumvoll, M., Villringer, A., Turner, R., 2010. Eigenvector centrality mapping for analyzing connectivity patterns in fMRI data of the human brain. PLoS One 5, e10232.
Mathew, R., Bak, T.H., Hodges, J.R., 2011. Diagnostic criteria for corticobasal syndrome: a comparative study. J. Neurol. Neurosurg. Psychiatry jnnp-2011-300875.
McKhann, G.M., Knopman, D.S., Chertkow, H., Hyman, B.T., Jr, C.R., Jack, Kawas, C.H., Klunk, W.E., Koroshetz, W.J., Manly, J.J., Mayeux, R., 2011. The diagnosis of dementia due to Alzheimer's disease: recommendations from the national institute on aging-Alzheimer's association workgroups on diagnostic guidelines for Alzheimer's disease. Alzheimer's Dement. 7, 263–269.
Meyer, S., Mueller, K., Stuke, K., Bisenius, S., Diehl-Schmid, J., Jessen, F., Kassubek, J., Kornhuber, J., Ludolph, A.C., Prudlo, J., 2017. Predicting behavioral variant frontotemporal dementia with pattern classification in multi-center structural MRI data. NeuroImage Clin. 14, 656–662.
Mueller, K., Jech, R., Bonnet, C., Tintěra, J., Hanuška, J., Möller, H.E., Fassbender, K., Ludolph, A., Kassubek, J., Otto, M., 2017. Disease-specific regions outperform whole-brain approaches in identifying progressive supranuclear palsy: a multicentric MRI study. Front. Neurosci. 11, 100.
Murphy, K., Birn, R.M., Handwerker, D.A., Jones, T.B., Bandettini, P.A., 2009. The impact of global signal regression on resting state correlations: are anti-correlated networks introduced? Neuroimage 44, 893–905.
Murray, R., Neumann, M., Forman, M., Farmer, J., Massimo, L., Rice, A., Miller, B., Johnson, J., Clark, C., Hurtig, H., 2007. Cognitive and motor assessment in autopsy-proven corticobasal degeneration. Neurology 68, 1274–1283.
Noble, S., Scheinost, D., Constable, R.T., 2019. A decade of test-retest reliability of functional connectivity: a systematic review and meta-analysis. Neuroimage 203, 116157.
Parmera, J.B., Rodriguez, R.D., Neto, A., Studart, Nitrini, R, Brucki, S.M.D., 2016. Corticobasal syndrome: a diagnostic conundrum. Dement. Neuropsychol. 10, 267–275.
Perron, O., 1907. On the theory of matrices. Math. Ann. 64, 248–263.
Pievani, M., Paternicò, D., Benussi, L., Binetti, G., Orlandini, A., Cobelli, M., Magnaldi, S., Ghidoni, R., Frisoni, G.B., 2014. Pattern of structural and functional brain abnormalities in asymptomatic granulin mutation carriers. Alzheimer's Dement. J. Alzheimer's Assoc. 10, S354–S363 e351.
Power, J.D., Barnes, K.A., Snyder, A.Z., Schlaggar, B.L., Petersen, S.E., 2012. Spurious but systematic correlations in functional connectivity MRI networks arise from subject motion. Neuroimage 59, 2142–2154.
Rakotomamonjy, A., Bach, F.R., Canu, S., Grandvalet, Y., 2008. SimpleMKL. J. Mach. Learn. Res. 9, 2491–2521.
Rebeiz, J.J., Kolodny, E.H., Richardson, E.P., 1968. Corticodentatonigral degeneration with neuronal achromasia. Arch. Neurol. 18, 20–33.
Schrouff, J., Rosa, M.J., Rondina, J.M., Marquand, A.F., Chu, C., Ashburner, J., Phillips, C., Richiardi, J., Mourao-Miranda, J., 2013. PRoNTo: pattern recognition for neuroimaging toolbox. Neuroinformatics 11, 319–337.
Seeley, W.W., Crawford, R.K., Zhou, J., Miller, B.L., Greicius, M.D., 2009. Neurodegenerative diseases target large-scale human brain networks. Neuron 62, 42–52.
Smith, R., Schöll, M., Widner, H., van Westen, D., Svenningsson, P., Hägerström, D., Ohlsson, T., Jögi, J., Nilsson, C., Hansson, O., 2017. In vivo retention of 18 F-AV-1451 in corticobasal syndrome. Neurology 89, 845–853.
Upadhyay, N., Suppa, A., Piattella, M.C., Giannì, C., Bologna, M., Stasio, F., Di, Petsas, N., Tona, F., Fabbrini, G., Berardelli, A., 2017. Functional disconnection of thalamic and cerebellar dentate nucleus networks in progressive supranuclear palsy and corticobasal syndrome. Parkinsonism Relat. Disord. 39, 52–57.
Warren, J.D., Rohrer, J.D., Schott, J.M., Fox, N.C., Hardy, J., Rossor, M.N., 2013. Molecular nexopathies: a new paradigm of neurodegenerative disease. Trends Neurosci. 36, 561–569.
Whitwell, J.L., Jack, C., Boeve, B.F., Parisi, J.E., Ahlskog, J., Drubach, D., Senjem, M., Knopman, D.S., Petersen, R.C., Dickson, D.W., 2010. Imaging correlates of pathology in corticobasal syndrome. Neurology 75, 1879–1887.
Woo, C.-W., Chang, L.J., Lindquist, M.A., Wager, T.D., 2017. Building better biomarkers: brain models in translational neuroimaging. Nat. Neurosci. 20, 365.
Zhou, J., Greicius, M.D., Gennatas, E.D., Growdon, M.E., Jang, J.Y., Rabinovici, G.D., Kramer, J.H., Weiner, M., Miller, B.L., Seeley, W.W., 2010. Divergent network connectivity changes in behavioural variant frontotemporal dementia and Alzheimer's disease. Brain 133, 1352–1367.